applied sciences

MDPI

Article

Study on the Fracture of a Shield Segment in a Fully Excavated Hard Rock Section under the Influence of Construction Loads

Cheng Zhu [1,2], Bin Zheng [3], Guoping Ren [1], Tugen Feng [1,*], Xiaochun Zhong [1] and Siyuan Huang [1]

1 College of Civil and Transportation, Hohai University, No.1 Xikang Road, Nanjing 210024, China; 2jsai299@hhu.edu.cn (S.H.)
2 China Communications Construction Company Limited Rail Transit Division, Beijing 101300, China
3 College of Mechanics and Materials, Hohai University, Nanjing 210024, China
* Correspondence: tgfeng75@163.com

Abstract: In this paper, the initiation of the fracture of a segment caused by the pressure of the jack and other factors during shield construction is discussed. Based on the Rots model in the finite element software Diana 10.4, the fracture width is solved. Combined with in situ measurements, the mechanisms of concrete fracturing of a segment under external loads, such as the jack thrust deflection angle and uneven jack thrust caused by the changes in the segment due to the upward buoyancy and shield attitude, are studied; additionally, the occurrence conditions and engineering control measures for segment fracture are summarized. The results show that when the attitudes of the shield and segment are identical, the total thrust of the shield is recommended not to exceed 21,000 kN, and is strictly limited to 24,000 kN. When the attitude inclination angle between the shield machine and the segment is less than 1°, the impact on the segment quality is small. When the inclination angle reaches 2°, the total thrust of the shield is recommended not to exceed 16,000 kN, and is strictly limited to 18,000 kN. When the inclination reaches 3°, a fracture is easily produced. When the total thrust is 19,000 kN, it is recommended that the loading increase or decrease in the left and right four grippers should not exceed 20%, and they are prohibited to exceed 30%. The fracture width increases exponentially with the increase in misalignment between adjacent segment rings. These research results provide a theoretical basis for jack pressure control during shield construction.

Keywords: shield tunnel; segment fracture; jack thrust; fracture width; segment misalignment

Citation: Zhu, C.; Zheng, B.; Ren, G.; Feng, T.; Zhong, X.; Huang, S. Study on the Fracture of a Shield Segment in a Fully Excavated Hard Rock Section under the Influence of Construction Loads. *Appl. Sci.* **2024**, *14*, 4102. https://doi.org/10.3390/app14104102

Academic Editor: Stefano Invernizzi

Received: 10 April 2024
Revised: 29 April 2024
Accepted: 30 April 2024
Published: 12 May 2024

1. Introduction

The reinforced concrete segment is the main supporting structure of a shield tunnel. Fracture not only affects the normal use of the supporting structure but also significantly reduces the impermeability and frost resistance of components. An excessively wide fracture will accelerate the corrosion of steel bars, thus reducing the bearing capacity of components and often causing serious safety hazards [1–3]. Due to the many adverse effects of fractures, China spends considerable manpower and financial resources on the prevention and repair of segment fractures every year, resulting in enormous economic losses and resource waste. Therefore, research on the mechanism of segment fracture elucidates not only the objective process but also how to respond to this process, which has great scientific and engineering significance.

Reinforced concrete has a multiphase composition of composite materials with complex, diverse properties; thus, its uniformity is poor, and its tensile strength is much lower than its compressive strength, resulting in reinforced concrete structures generally forming fractures. Therefore, fracturing of reinforced concrete structures is inevitable, and it is difficult to control the degree of harm to be within a permissible range. Therefore, the calculation of fracture width is of great practical significance to the evaluation, identification and maintenance of structures. Research on the width of a fracture under load [4] has been carried out abroad. The bond slip theory was first proposed by Saliger [5] in 1936 from the experimental study of axial tension rods. The bond slip theory assumes that the fracture width of components is equal to the deformation difference between the reinforcement and concrete within the range of the fracture spacing and provides the calculation formula for the average fracture width. In the 1960s, Broms [6,7] and other researchers denied the idea that the fracture width in the bond slip theory is equal to the deformation difference between the reinforcement and concrete through a series of tests and put forward the theory of unbonded slip. In 1968, Gergely and Lutz [8] proposed the Gergely and Lutz formula through regression analysis based on their test results. In 1971, Goto [9] proposed that the shape of a steel bar has an effect on the fracture width in a reinforced concrete component. Later scholars combined bond slip theory with nonbond slip theory to obtain a comprehensive theory, which not only considers the significant effect of the distance from the surface of the member to the reinforcement bar on the fracture width but also includes the influence of bond slip. The former Soviet Union Reinforced Concrete Research Institute, the American Concrete Association (ACI), the British Cement and Concrete Association (CCA), the European Concrete Association International Prestress Association (CEB-FIP), the Southeast University, Dalian University of Technology, China Academy of Architectural Sciences, etc., have carried out research on fracture width calculation. The achievements of the above scholars and research institutions have been compiled to determine the relevant design specifications. For example, the domestic Code for Design of Concrete Structures [10] adopts this comprehensive research theory.

However, the mechanical behavior of a segment lining fracture in a shield tunnel is not explained by the above methods. The reinforced concrete segment is the main supporting structure in a shield tunnel. Fractures caused by deformation are very common and may occur from the production period to the construction period and operation period. In addition to affecting the normal use of the supporting structure, fractures also significantly reduce the impermeability and frost resistance of the component. Excessively wide fractures will accelerate the corrosion of the steel bar and then reduce the bearing capacity of the component, which often causes serious safety hazards. To address the aforementioned issues, Xu [11] proposed an improved model incorporating internal pressure, crack width, and failure modes, aiming to provide a more precise estimation of the bond strength between deformed bars embedded in concrete under various crack cases. In view of the behavior of fractures in reinforced concrete segments used in shield tunnels, the Code for Design of Segments for Shield Tunnels [12] compiled in Japan has systematically proposed empirical formulas for fracture width calculation based on cake-slip theory, but the values of some variables are not clearly expressed. Due to the complexity of factors affecting the fracture width of segments, it is difficult to establish a universally applicable fracture width calculation formula, which needs to be improved using finite element analysis. The finite element analysis of reinforced concrete structures is performed by combining the finite element analysis method and the mechanical properties of the reinforced concrete. Since the research on reinforced concrete is based on many test results and the complexity and high cost of tests restrict the development of fracture research on reinforced concrete structures, the use of finite element and other numerical methods to analyze the mechanical properties of reinforced concrete structures has become a research focus. The effect of crack width on the corrosion rate of reinforcement was numerically analyzed by Xu [13]. The segment simulations were directed at investigating concentrated loading, representative of the jack thrust force applied while installing the segments during the tunnel boring machine (TBM) installation phase [14]. A numerical investigation is conducted here to study the mechanical behavior of continuous-joint shield tunnels, strengthened by the SPCC strengthening technique [15].

The Mohr–Coulomb failure criterion was used in early finite element analysis, but later studies showed that the polygonal cone could not accurately reflect the failure surface of concrete. In terms of the constitutive relationship of concrete, scholars from various countries have proposed various models, such as those based on linear elastic theory [16], nonlinear elastic theory [17], elastic–plastic theory [18], internal time theory [19], viscoelastic theory [20] and viscoplastic theory [21]. However, due to the complex characteristics of concrete materials, there is no recognized theory that can be widely applied to concrete structures under various conditions. The combination of reinforcement and concrete is an important problem in the finite element analysis of steel and concrete. In the early days of related research, steel bars and concrete were divided into small units for calculation, but this approach is not suitable for large structures and three-dimensional analysis. Later, Schnobrich WC [22] in the United States proposed an integral steel bar model, which transforms steel bars into equivalent concrete and calculates their properties according to a unified stiffness matrix. This model is more suitable for the analysis of large concrete structures.

The simulation of bond slip between steel bars and reinforced concrete is a difficult problem in the finite element analysis of reinforced concrete structures. After long-term research and development, scholars have proposed a variety of bond units, such as double-spring bond units, quadrilateral slip units, and contact units. The bond slip model has also developed from an early linear model to a nonlinear model and continues to improve.

The simulation of fracture width is always a difficult problem in the finite element analysis of reinforced concrete structures. Because the occurrence of fractures makes concrete discontinuous and the basic principle of finite elements comes from continuum mechanics, it is difficult to simulate the cracking behavior of concrete accurately. To solve this problem, scholars have proposed a variety of fracture simulation methods, such as the diffuse cracking method and discrete cracking method. The dispersion cracking method assumes that the elements will not separate and that cracking is expressed by strain. The discrete cracking method assumes that the elements will be separated, and interface elements are added between them. The limitation of the discrete cracking method is that the location of cracking needs to be known, whereas diffuse cracking is more general. The dispersion cracking method is proposed based on the fracture zone theory [23], which can be summarized as describing the mechanical behavior of the whole process of fracture cracking through fracture energy.

In summary, domestic and foreign specifications have put forward clear requirements for the fracture width of reinforced concrete structures, and there are many factors affecting the emergence and development of fractures. Thus, it is difficult to develop a universally applicable formula. At the same time, the existing numerical research results [24,25] are all based on the stress–cracking strain curve of concrete, which can only obtain the segment cracking strain and cannot quantitatively reflect the fracture width; thus, it cannot be checked directly based on the structural design specification of a "fracture width checking calculation". It cannot reflect the fracture width quantitatively and cannot be checked directly based on the structural design specification "fracture width checking calculation". Therefore, based on the Rots model in the finite element software Diana 10.4, this paper explores the effects of the jack thrust magnitude, a thrust direction change, an uneven allowance of cylinder pressure and buoyancy on the segment fracture width and compares the results with observations from actual engineering practice. Based on this, the cracking empirical formula of segments in the Japanese Code for the Design of Segments for Shield Tunnels is optimized to provide a research basis for similar projects.

2. Research and Analysis of the Cracking Mechanism

During the construction phase of shield tunnels, the causes of segment cracking are mainly the magnitude of the jack thrust, a change in the thrust direction, the nonuniform distribution of cylinder pressure, and the occurrence of segment misalignment [26,27]. As shown in Figures 1 and 2, when the jack thrust F_1 exceeds the segment's ultimate bearing capacity or segment attitude deviation occurs, the segment will crack to different degrees. In addition to the small linear radius of the tunnel design, other reasons leading to the abnormal attitude deviation of the segment are as follows: (1) there is a certain inclination angle between the thrust direction of the and normal direction of the segment torus, and the tangential component force F_3 produces a moment M; (2) the cylinder exerts uneven pressure on the segment; (3) misalignment of the segment occurs. Therefore, in view of segment fracture control, both domestic and foreign codes put forward clear requirements based on the fracture width of reinforced concrete structures. In addition, 16 loading cylinders at the site are divided into four zones, which are represented by four colored arrows in Figure 1.

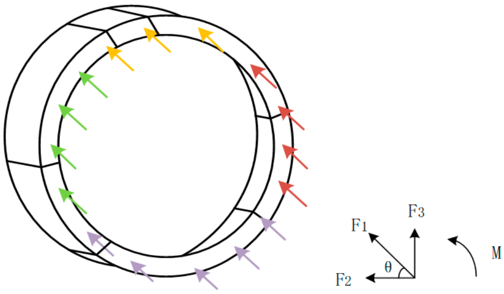

Figure 1. The nonuniform thrust produces a certain inclination angle with the normal of the torus of the segment.

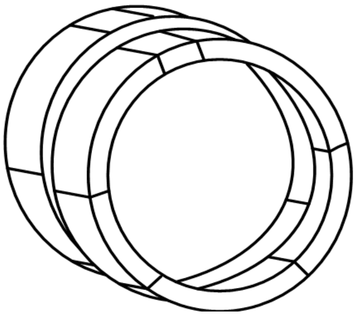

Figure 2. The segment is misaligned.

According to the introduction above, the existing numerical research results [24,25] cannot quantitatively reflect the fracture width value, and the calculation results cannot be checked directly based on the structural design specification "fracture width checking calculation". Therefore, the fracture "bandwidth" is introduced in this paper to quantitatively describe the w-ε_{cr} relationship, as shown in Equation (1).

$$h_c = \frac{w}{\varepsilon_{cr}} \tag{1}$$

where h_c is the fracture "bandwidth", representing the standard distance of the dispersion from the fracture width w to the cracking strain ε_{cr}.

The finite element analysis software Diana adopted in this paper provides three methods for describing the fracture "bandwidth": (1) the Rots model; (2) the Govindjee model; and (3) user-specified values. The Rots model determines the fracture "bandwidth" based on the cell size, and the Govindjee model determines the fracture "bandwidth" based on the cracking direction. Since the direction of segment cracking is unknown, the cell size is set to 0.5 m during meshing. Therefore, the Rots model is adopted in this paper to determine the fracture "bandwidth".

3. Establishment of a Prediction Model of Segment Fracture Width

3.1. The Establishment of Geometric Models

A geometric model is established based on the working conditions and segment dimension parameters of the October Square Station and Jinling Petrochemical Station of Nanjing Metro Line 6. The ground elevation of the working area is approximately 16.57–35.59 m, and the main strata through the section are moderately weathered argillaceous sandstone, silty clay and silty clay, strongly weathered andesite and moderately weathered andesite.

The strength of the rock strata is 10–80 MPa, and the quartz content of the argillaceous sandstone is 40–50%. The upper soft and lower hard strata account for approximately 16%, the soil layer accounts for approximately 10%, and the rock layer accounts for approximately 74%. Groundwater has no influence on the construction of the work area. The physical and mechanical parameters of each rock and soil layer are listed in Table 1.

Table 1. Physical and mechanical parameters of each rock and soil layer.

Layer	Density (kN/m^3)	Modulus of Elasticity (MPa)	Cohesive Force (MPa)	Angle of Internal Friction	Poisson's Ratio
Silty clay	19.29	5.97	3.26×10^{-2}	11.7	0.33
Andesite	26.49	3.1×10^3	0.4	35	0.23
Argillaceous sandstone	26.29	5.5×10^3	0.4	35	0.23

The size parameters of the segment are as follows: inner diameter 5500 mm, outer diameter 6200 mm, and ring width 1200 mm. The parameters of the segment structure are as follows: splicing block F, adjacent blocks L1 and L2, and standard blocks B1, B2 and B3. The center angle corresponding to the splicing block is 21.5°, and the center angles corresponding to the adjacent block and the standard block are 68° and 67.5°, respectively. The segment material is high-strength concrete with an elastic modulus of 3.45×10^4 MPa, a Poisson's ratio of 0.2, density of 2500 kg/m^3, a tensile strength of 1.89 MPa and a breaking energy of 147.6 N/m [24]. The segment design and a model diagram are shown in Figures 3 and 4.

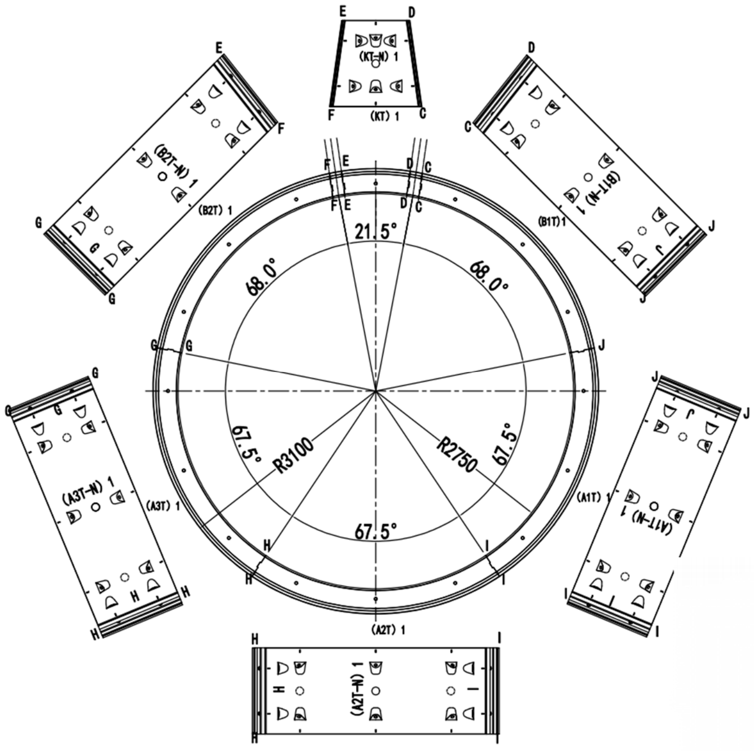

Figure 3. Segment size parameter design drawing.

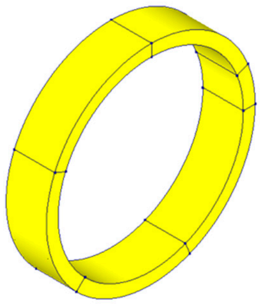

Figure 4. Segment model.

The internal steel mesh of standard block B1 of the segment is shown in Figure 5. There are 20 inner annular ribs and 106 longitudinal ribs of a single-ring segment, as shown in Figure 6. The steel bars are grade 3 steel with a diameter of 16 mm and an elastic modulus of 200 GPa.

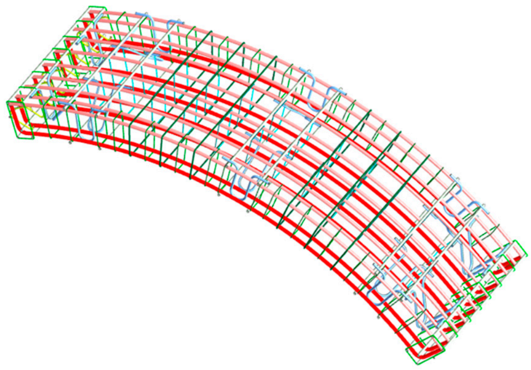

Figure 5. Diagram of the internal steel mesh of standard block B1 of the segment.

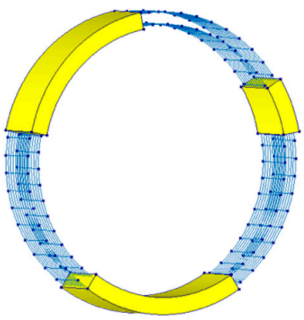

Figure 6. Steel mesh modeling.

3.2. Setting of Contact Surface

The X direction is specified as the shield driving direction, and rings A, B and C are located along the X directions, as shown in Figure 7. It is assumed that ring A has been grouted but the slurry has not solidified, that ring B is located in the shield tail brush, which is displayed by green dots in Figure 8 and that ring C is subject to the thrust of the jack. Rings A and B constrain the translation and rotation of XYZ in three directions. The interaction between the torus of ring B and the shield tail brush is simulated by the boundary interface, the normal stiffness of the boundary interface material is 2×10^8 N/m^3, and the shear stiffness is 2×10^7 N/m^3, as shown in Figure 8.

The girth and longitudinal joints of the segment are connected with class 8.8 ordinary bolts and class 8.0 nuts. Interface elements are used to simulate the joints. The normal stiffness of the sides of the interface elements is 1×10^{10} N/m^3, and the shear stiffness is 1×10^9 N/m^3. The girth and longitudinal joints are shown in Figures 9 and 10, respectively.

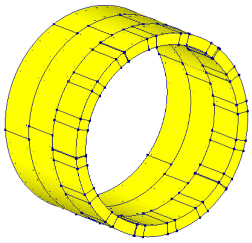

Figure 7. Variation in diffusion parameters with grouting pressure.

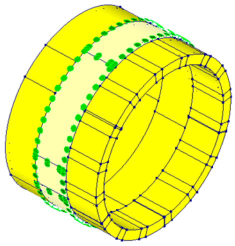

Figure 8. Shield tail brush restraint.

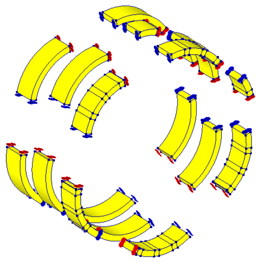

Figure 9. Girth joints.

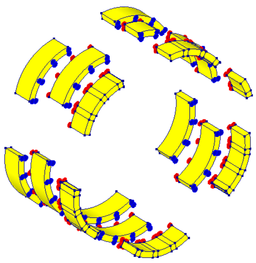

Figure 10. Longitudinal joints.

3.3. Load Setting

This paper mainly discusses the effects of jack thrust, the change in gripper angle, the nonuniform distribution of cylinder pressure and buoyancy on the segment crack width. In the field test, the jack exerted force on the segment through 16 grippers, and the area of a single gripper was 0.1 m^2. When the influence of jack thrust on fracture width is analyzed, the direction of thrust exerted by 16 grippers on the segment is consistent with the normal direction of the annular plane of the segment, as shown in Figure 11. When the influence of the change in the gripper angle on the fracture width is analyzed, two thrust components are set along the normal and tangential directions of the gripper torus so that a certain angle is formed between the total thrust direction and normal direction of the gripper torus. When the influence of the nonuniform distribution of cylinder pressure on the segment fracture width is investigated, the thrust forces of the left and right eight grippers are increased or decreased along the central axis of the torus. When exploring the influence of segment misalignment on the fracture width, forced displacement is applied to the segment with the shield tail brush removed, as shown in Figure 12.

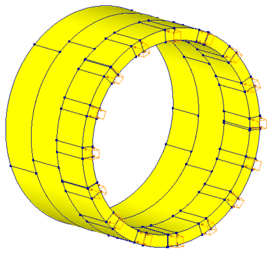

Figure 11. The grippers apply thrust.

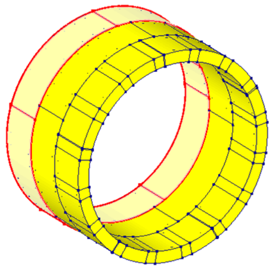

Figure 12. A forced displacement is applied to the shield tail brush segment.

In the numerical calculation, the Newton–Raphson method and arc length method of from the Diana software were used. The load step adopted the custom mode, the step size setting range was 10–100, the convergence criterion was controlled by the energy method in the balance iteration, and the collection tolerance was set to 0.5.

4. Analysis of Factors Influencing Segment Fracture Width

4.1. Comparative Analysis between the Numerically Simulated Fracture Generation and Field-Observed Fracture Generation

The test target segment field test is located in the section between the October Square Station and Jinling Petrochemical Station of Nanjing Metro Line 6. Ten rings (2365, 2370, 2380, 2389, 2405, 2411, 2428, 2436, 2458 and 2460 rings) were selected from the straight section rings 2365–2460 according to the driving parameters. There are thirty-two propulsion oil cylinders at the tail of the shield and sixteen grippers (one gripper for every two oil cylinders). Therefore, the segment torus is subject to the thrust of 16 grippers during propulsion, which are divided into four colored zones displayed in Figure 13, and the thrust direction and normal inclination angle of the segment torus range from 0.5° to 1°. In actual propulsion, the sixteen grippers are controlled by four regions: the upper three grippers are interconnected, the lower five grippers are linked and the left and right four grippers are linked.

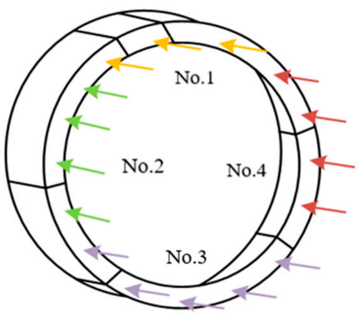

Figure 13. Cylinder control area.

In the numerical simulation, 16 grippers loading surfaces are divided on the C ring, and the torus is divided into 32 pieces. To more accurately display the fracture width values in different directions, a local coordinate system was established for each piece according to the central angle of the circle. For example, the red block in Figure 14 was set as the 45° axis in the y direction and 135° axis in the z direction.

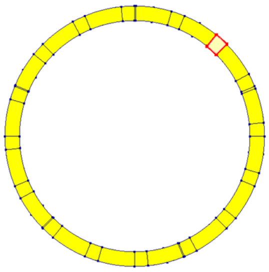

Figure 14. The 45° direction segment.

In the Diana software, the von Mises equivalent strain ε_{eq} was used to represent the fracture width. The equivalent strain ε_{eq} was defined as follows:

$$\varepsilon_{eq} = \frac{2}{3}\sqrt{\frac{3\left(e_{xx}^2 + e_{yy}^2 + e_{zz}^2\right)}{2} + \frac{3\left(\gamma_{xy}^2 + \gamma_{yz}^2 + \gamma_{zx}^2\right)}{4}} \tag{2}$$

$$\begin{aligned} e_{xx} &= \tfrac{2}{3}\varepsilon_{xx} - \tfrac{1}{3}\varepsilon_{yy} - \tfrac{1}{3}\varepsilon_{zz} \\ e_{yy} &= -\tfrac{1}{3}\varepsilon_{xx} + \tfrac{2}{3}\varepsilon_{yy} - \tfrac{1}{3}\varepsilon_{zz} \\ e_{zz} &= -\tfrac{1}{3}\varepsilon_{xx} - \tfrac{1}{3}\varepsilon_{yy} + \tfrac{2}{3}\varepsilon_{zz} \end{aligned} \tag{3}$$

where e_{xx}, e_{yy} and e_{zz} represent destructive strains in three orthogonal directions; ε_{xx}, ε_{yy} and ε_{zz} represent axial strains; γ_{xy}, γ_{yz} and γ_{zx} represent tangential strains. The simulated values of the fracture width of the target ring tube are listed in Table 2.

Table 2. Simulated value of fracture width of segment numbered 2365–2460 (mm).

Number	Inclination Angle (°)	Upper Subdivision (MPa)	Left Part (MPa)	Subdivision (MPa)	Right Part (MPa)	Total Thrust (kN)	ε_{eq} (mm)
Ring 2365	0.6	8.2	11.6	15.4	8.9	18,360	0.13
Ring 2370	0.6	12.7	10.8	10.2	8.4	16,590	0.13
Ring 2380	0.5	9.8	12.1	16.3	10.9	20,290	0.15
Ring 2389	1	12.7	9.4	13.8	12.7	19,550	0.44
Ring 2405	0.6	10.9	8.6	16.4	9.8	18,830	0.14
Ring 2411	0.6	9.9	11.4	16.7	11	20,280	0.15
Ring 2428	0.7	10.6	14.8	15.5	11.9	21,610	0.43
Ring 2436	0.6	9.9	12.2	16.0	11.6	20,490	0.14
Ring 2458	0.6	8.9	10.2	15.7	11.3	19,120	0.15
Ring 2460	0.6	10.9	11.2	16.4	11.7	20,630	0.15

No significant fractures appeared in the segments of ring 2365 and ring 2370, while the other segments showed significant fractures. The concrete design specification requires that the fracture width should not exceed 0.2 mm. At the same time, some studies [28] have shown that when the fracture width does not exceed 0.15 mm, it will have little impact on the structure and even heal itself. When the fracture width exceeds 0.15 mm, it may continue to develop. The simulation results of the fracture widths of rings 2380, 2389, 2411, 2428, 2458 and 2460 are 0.15–0.2 mm, as shown in Table 2, indicating that the numerical modeling in this paper is reasonable and effective. The numerical simulation and field test results are shown in Figure 15.

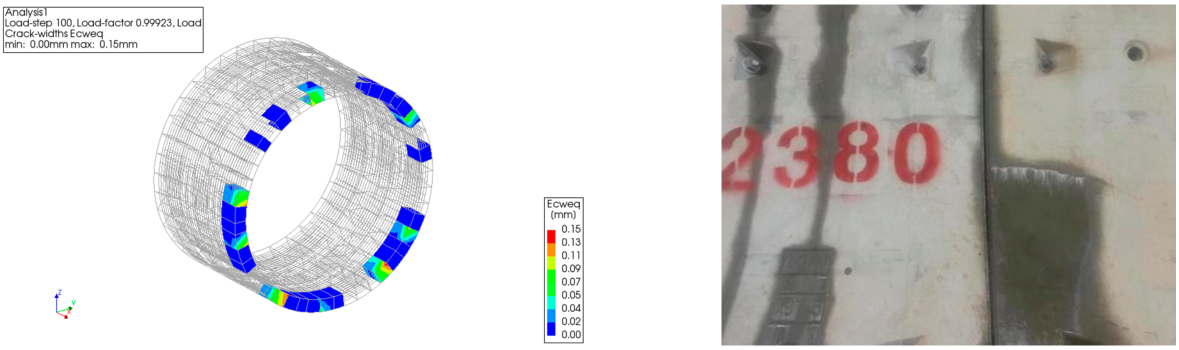

(**a**) Ring 2380 (5 o'clock direction).

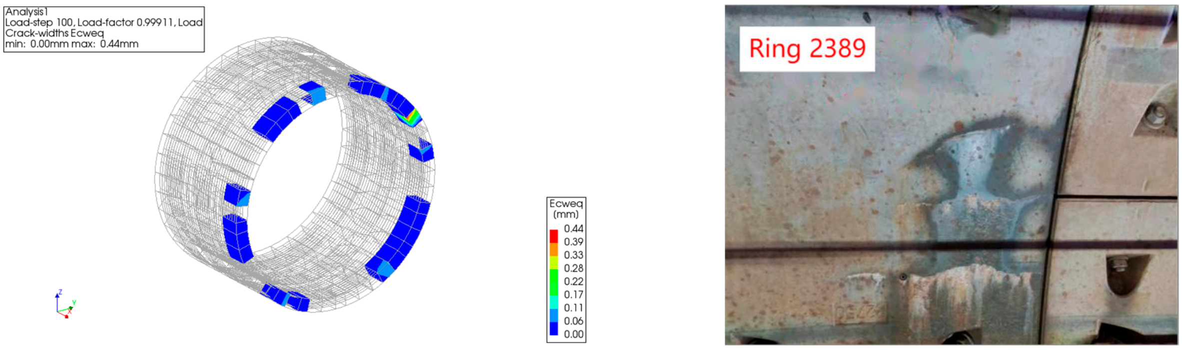

(**b**) Ring 2389 (10 o'clock direction).

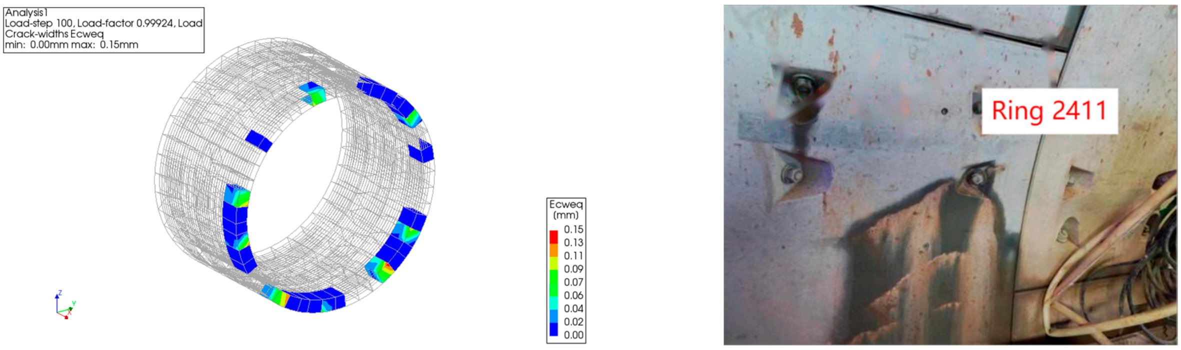

(**c**) Ring 2411 (5 o'clock direction).

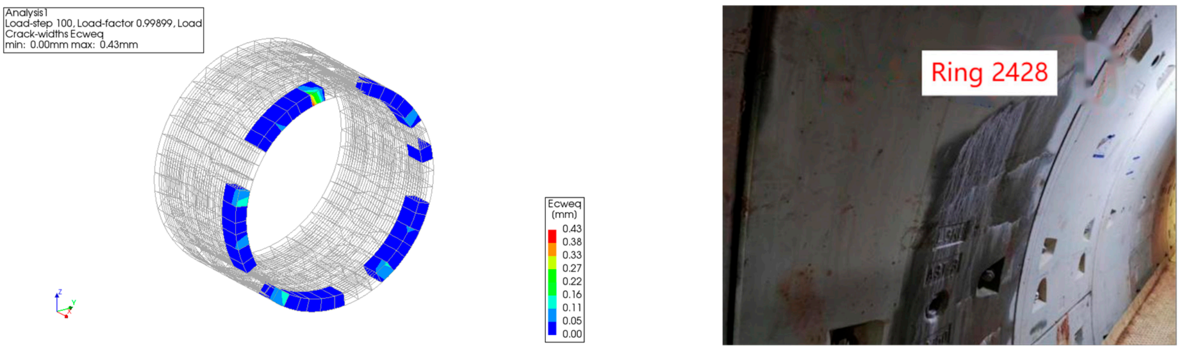

(**d**) Ring 2428 (3 o'clock direction).

Figure 15. *Cont*.

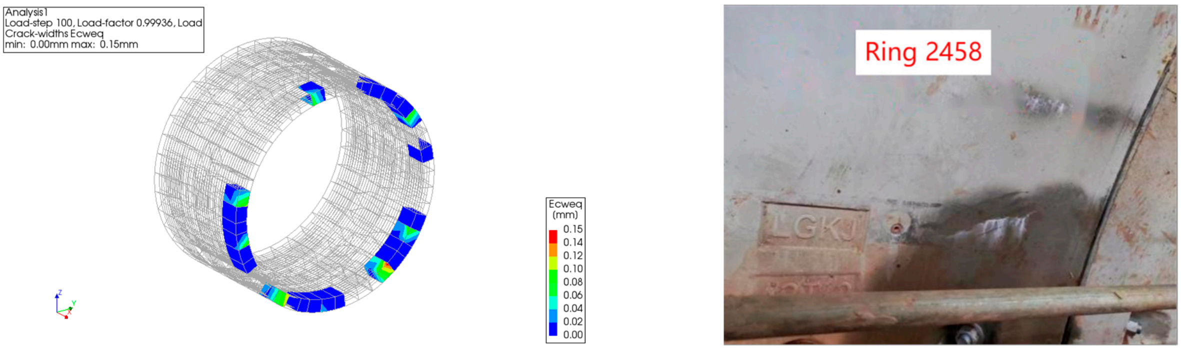

(**e**) Ring 2458 (5 o'clock direction).

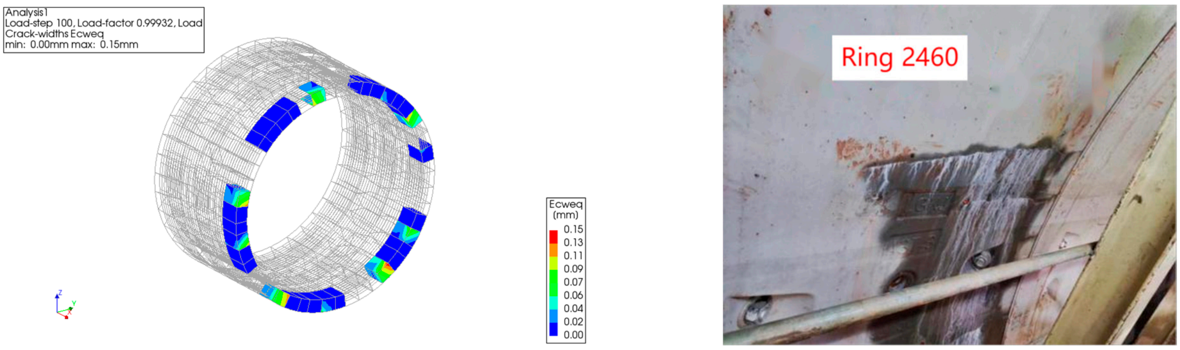

(**f**) Ring 2460 (5 o'clock direction).

Figure 15. Numerical simulation figure of segment cracking and field test results.

As shown in Figure 15a,c,e,f, the crack width in the 5 o'clock direction in the segment in the simulation cloud image is 0.15 mm, and significant cracks appeared in the 5 o'clock direction in rings 2380, 2411, 2458 and 2460 in the field test. As shown in Figure 15b,d, crack widths in the 10 o'clock direction in the segment in the simulation cloud image are 0.44 mm and 0.43 mm, and several significant cracks appeared in the 10 o'clock direction in rings 2389 and 2428 in the field tests. It can be seen that segment cracks are prone to appearing at the 5 and 10 points.

4.2. Effect of Thrust Magnitude on the Fracture Width of a Segment

Table 2 shows that when the total thrust is close to 20,000 kN, the fracture width of the segment in the field test is close to the standard limit value of 0.2 mm. This section further explores the influence of thrust magnitude on the fracture width of segments. The total thrust is set to 20,000–24,000 kN. The simulation results for the axial, tangential and equivalent fracture widths of the segment are listed in Table 3. The simulated figures of the equivalent fracture widths with different total thrusts are shown in Figure 16.

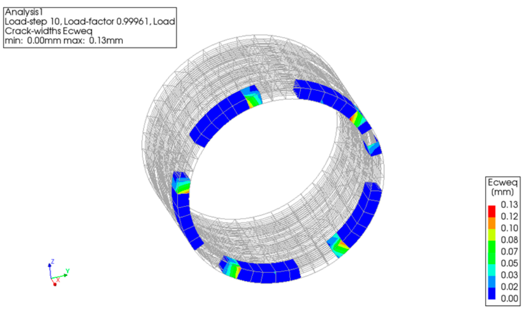

(**a**) P = 20,000 kN.

Figure 16. *Cont.*

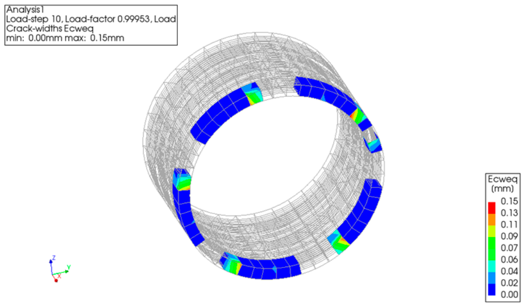

(**b**) P = 21,000 kN.

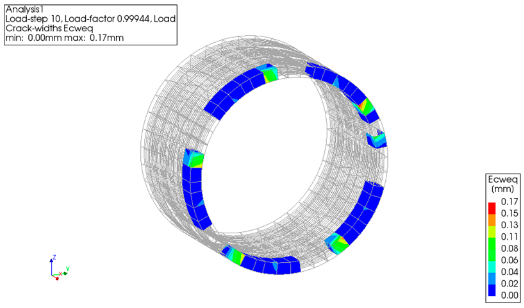

(**c**) P = 22,000 kN.

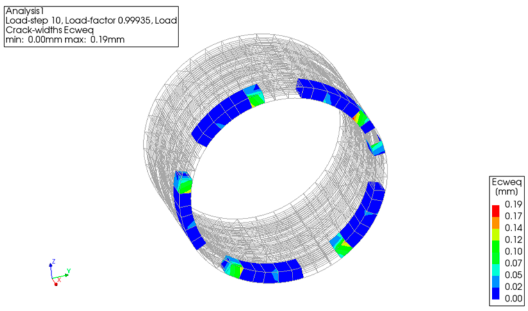

(**d**) P = 23,000 kN.

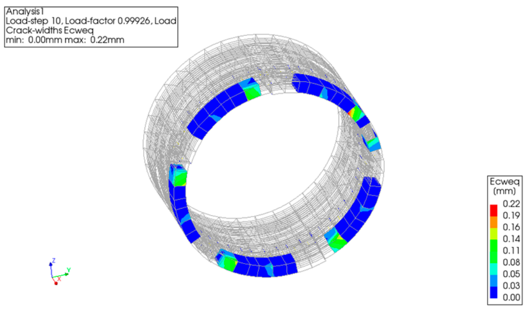

(**e**) P = 24,000 kN.

Figure 16. Numerical simulation figure of fracture width under total thrust 20,000–24,000 kN.

Table 3. Simulation value of fracture width of segment with total thrust of 20,000–24,000 kN (mm).

Total Thrust/kN	ε_{xx}	ε_{yy}	ε_{zz}	γ_{xy}	γ_{yz}	γ_{zx}	ε_{eq}
20,000	0.004	0.13	0.008	0.02	0.02	0.004	0.13
21,000	0.004	0.15	0.01	0.02	0.02	0.005	0.15
22,000	0.005	0.17	0.02	0.02	0.03	0.006	0.17
23,000	0.006	0.19	0.03	0.02	0.03	0.007	0.19
24,000	0.007	0.23	0.03	0.03	0.04	0.007	0.22

As shown in Figure 16e, when the total thrust reaches 24,000 kN, the equivalent fracture width is 0.22 mm. Based on the empirical Equation (4) of segment cracking in Japan's Code for Tunnel Design, the maximum spacing of segment distribution ribs under the total thrust of 20,000–24,000 kN can be calculated, which is listed in Table 4, where $L_{\max}$ is calculated according to the Code for Design of segment of Shield Tunnels prepared by Japan [10]:

$$w = L_{\max} \cdot \left(\frac{\sigma_{se}}{E_s} + \varepsilon'_{csd} \right) \tag{4}$$

where $L_{\max}$ is the maximum interval (mm) of the distributed steel bars, and the lower limit is $0.51L_1$. L_1 is calculated according to Equation (5):

$$L_1 = 1.1 \cdot k_1 \cdot k_2 \cdot k_3 \cdot \{4c + 0.7 \cdot (c_s - \varphi)\} \tag{5}$$

where k_1 is the coefficient representing the influence of the steel bar surface shape on the fracture width, and a k_1 value of 1.0 is taken for the deformed steel bar. k_2 is the influence coefficient of concrete quality on fracture width, and $k_2 = \frac{15}{f'_c+20} + 0.7$. F'_c is the compressive strength of concrete (N/mm^2). k_3 is the coefficient that represents the influence of the number of steel layers under tension, and $k3 = \frac{5(n+2)}{7n+8}$. n is the number of layers of steel bars under tension. c is the thickness of the protective layer (mm). c_s is the center spacing of the rebar (mm). φ is the diameter of the steel bar (mm). σ_{se} is the increase in the stress of the bar (N/mm^2). E_s is the elastic modulus of the reinforcement (N/mm^2). To consider the increase in fracture width caused by concrete shrinkage and creep, $\varepsilon_{csd}{}'$ is generally equal to 1.5×10^{-8}.

Table 4. Calculation and simulation results of fracture width of segment with total thrust of 2000–24,000 kN.

Thrust (kN)	σ_{se} (MPa)	$L_{\max}$ (mm)	Fracture Width (mm)
20,000	0.69	2.3 L_1	0.13
21,000	1.59	2.3 L_1	0.15
22,000	2.17	2.4 L_1	0.17
23,000	2.71	2.5 L_1	0.19
24,000	3.95	2.5 L_1	0.22

In Equation (4), σ_{se} represents the increase in the stress of the steel bar. Since no specific solution equation is given, the maximum stress at the fracture of the segment is used instead in this paper. In Equation (1), $L_{\max}$ represents the maximum interval of the distributed steel bars, and the lower limit is 0.51 L_1. L_1 is calculated according to Equation (3). By comparing the calculation results with the simulation results, it can be concluded that the range of $L_{\max}$ is (2.3–2.5) L_1.

4.3. Effect of Thrust Magnitude on the Fracture Width of a Segment

In shield tunneling, when the attitudes of the shield machine and segment are inconsistent, the thrust direction and normal direction of the segment torus are not identical, and a tangential shear force will be generated on the segment ring, resulting in different degrees of fracture in the segment. The actual inclination angle between the two is generally between 0° and 2.5°. This section quantitatively describes the relationship between the inclination angle and fracture width when the inclination angle is 1°, 2° and 3°. The simulation results are listed in Table 5.

Table 5. Simulation results of fracture widths at different inclination angles.

Total Thrust P (kN)	Inclination Angle θ (°)	Equivalent Width ε_{eq} (mm)
16,000	1	0.03
	2	0.15
	3	0.27
17,000	1	0.08
	2	0.18
	3	0.35
18,000	1	0.13
	2	0.23
19,000	1	0.12
	2	0.28
20,000	1	0.17
	2	0.34

As shown in Table 5, when the inclination angle between the gripper and the normal direction of the segment torus is 1°, the thrust reaches 20,000 kN. The fracture width is still controllable. When the inclination angle between gripper and the normal direction of the segment torus is 2°, the segment fracture width will exceed the limit (0.23 mm) when the total thrust reaches 18,000 kN. When the inclination angle between gripper and the normal direction of the segment torus is 3°, the segment fracture width will exceed the limit (0.27 mm) when the total thrust reaches 16,000 kN. Therefore, the orientation of the gripper should be strictly controlled in shield tunneling to prevent too large a deflection angle between the thrust direction and segment normal direction. The simulated figure of fracture widths at different inclination angles are shown in Figure 17. When the inclination is 3° and the thrust is 16,000 kN, the crack width of the segment has exceeded the limit of 0.27 mm. When the inclination is 2° and the thrust is 18,000 kN, the crack width of the segment has exceeded the limit of 0.23 mm.

4.4. Influence of Nonuniform Distribution of Cylinder Pressure on the Fracture Width of a Segment

When the shield machine turns, the distribution of cylinder pressure needs to be adjusted. For example, when the shield machine makes a left turn, the extension of the cylinder in the left partition will be appropriately reduced, and the extension of the cylinder in the right partition will be increased, which corresponds to the reduction in the thrust of the cylinder in the left partition and the increase in the thrust of the cylinder in the right partition. The loading model diagram is shown in Figure 18. The red part is where the cylinder is loaded. This section analyzes the influence of uneven cylinder pressure distribution on segment fracture width. The numerical simulation results are listed in Table 6.

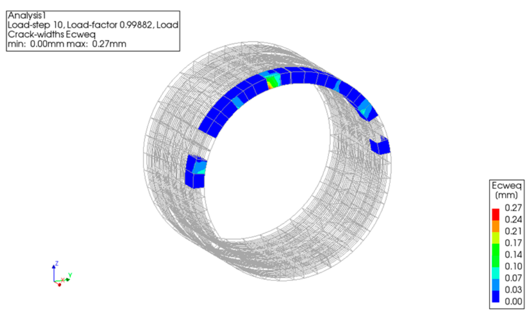

(**a**) P = 16,000 kN, θ = 3°.

Figure 17. *Cont.*

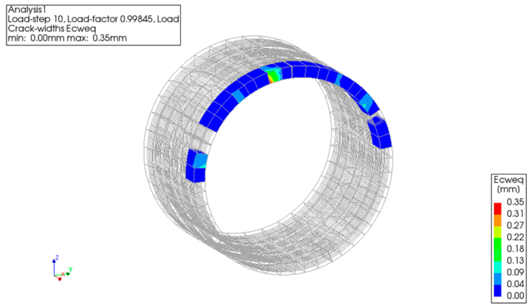

(**b**) P = 17,000 kN, θ = 3°.

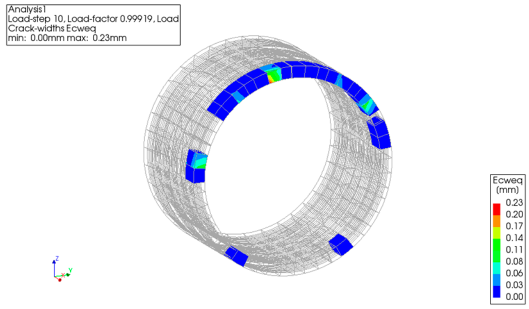

(**c**) P = 18,000 kN, θ = 2°.

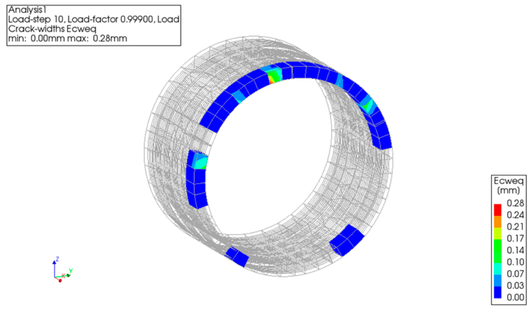

(**d**) P = 19,000 N, θ = 2°.

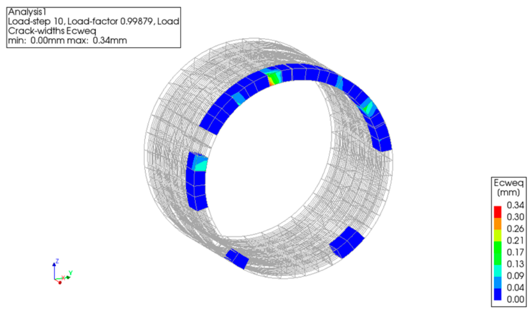

(**e**) P = 20,000 kN, θ = 2°.

Figure 17. Numerical simulation of fracture width at different inclination angles.

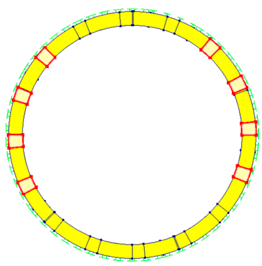

Figure 18. The left and right side partitions control 4 grippers, respectively.

Table 6. The simulation value of segment fracture width under the change of loading amplitude of the left and right 4 grippers.

Total Thrust (kN)	Left	Right	Equivalent Fracture Width (mm)
16,000	−10%	+10%	0.11
	−20%	+20%	0.12
	−30%	+30%	0.13
	−50%	+50%	0.23
17,000	−10%	+10%	0.12
	−20%	+20%	0.13
	−30%	+30%	0.14
	−40%	+40%	0.20
18,000	−10%	+10%	0.12
	−20%	+20%	0.14
	−30%	+30%	0.15
	−35%	+35%	0.20
19,000	−10%	+10%	0.13
	−20%	+20%	0.15
	−30%	+30%	0.21

Due to the action of gravity, the thrust force received by the lower five grippers is 1.5 times that of the other grippers. When the total thrust is 16,000 kN, the stress exerted by the lower five grippers on the segment is 12.975 MPa, and the stress exerted by the upper three grippers on the segment is 8.65 MPa. When the increase or decrease in the loading of the left and right four grippers is adjusted to 50%, the stress exerted on the segment by the four grippers on the left is 4.325 MPa, while the stress exerted on the segment by the four grippers on the right is 12.975 MPa. The equivalent crack width of the segment is 0.23 mm, which exceeds the standard limit value, as shown in Figure 19a.

When the total thrust is 17,000 kN, the stress exerted on the segment by the lower five grippers is 13.785 MPa, and the stress exerted on the segment by the upper three grippers is 9.19 MPa. When the increase or decrease in the loading of the left and right four grippers is adjusted to 40%, the stress exerted on the segment is 5.514 MPa. The stress exerted on the segment by the four grippers on the right is 12.866 MPa, and the equivalent crack width of the segment is 0.20 mm, reaching the standard limit value, as shown in Figure 19b.

When the total thrust is 18,000 kN, the stress exerted on the segment by the lower five grippers is 14.596 MPa, and the stress exerted on the segment by the upper three grippers is 9.73 MPa. When the increase or decrease in the loading of the left and right four grippers is adjusted to 35%, the stress exerted on the segment is 6.325 MPa. The stress exerted on the segment by the four grippers on the right is 13.136 MPa, and the equivalent crack width of the segment is 0.20 mm, which has exceeded the standard limit value, as shown in Figure 19c.

When the total thrust is 19,000 kN, the stress exerted on the segment by the bottom five grippers is 15.41 MPa, and the stress exerted on the segment by the top three grippers is 10.27 MPa. When the increase or decrease in the loading of the left and right four grippers is adjusted to 30%, the stress exerted on the segment is 7.189 MPa. The stress exerted on the segment by the four grippers on the right is 13.351 MPa, and the equivalent crack width of the segment is 0.21 mm, which has exceeded the standard limit value, as shown in Figure 19d.

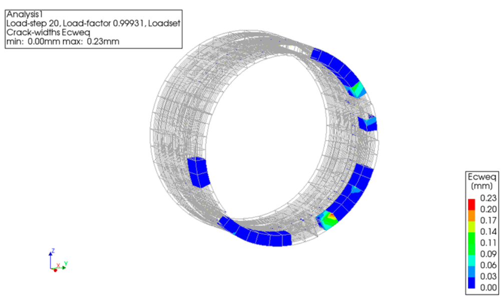

(**a**) P = 16,000 kN. Range of increase and decrease is 50%.

Figure 19. *Cont.*

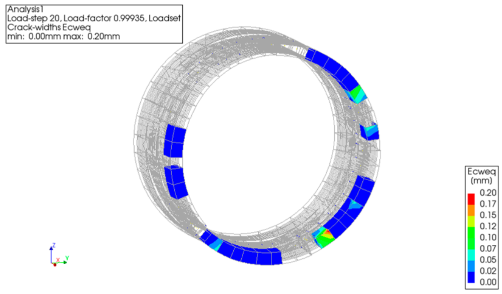

(**b**) P = 17,000 kN. Range of increase and decrease is 40%.

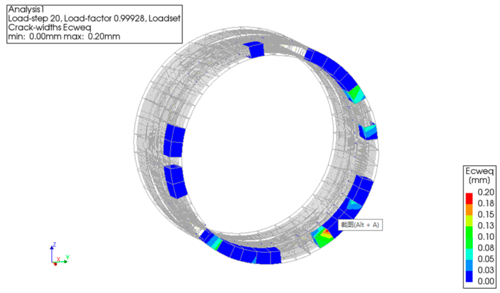

(**c**) P = 18,000 kN. Range of increase and decrease is 35%.

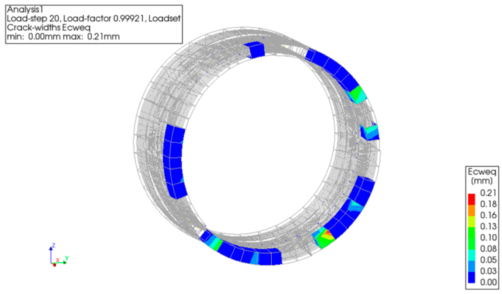

(**d**) P = 19,000 kN. Range of increase and decrease is 30%.

Figure 19. Numerical simulation figure of fracture width under different increase and decrease in grippers.

4.5. Influence of Segment Misalignment on Fracture Width

In a layer of water-rich hard rock, the segment will be mispositioned due to the greater buoyancy of the grouting slurry, and the amount of misalignment at the shield tail is small and gradually increases after the segment escapes from the shield tail. The relationship between the amount of segment misalignment and the fracture width is quantitatively investigated in this section. In the numerical modeling, it is assumed that rings A, B and C are all constrained by the spring of the slurry, the stiffness coefficient of the spring constraint is 3.9×10^7 N/m^3, and misalignment occurs between rings A and B and C, as shown in Figure 20. The red part is the A ring. Figure 21 shows a curve of the simulation results in terms of the relationship between segment misalignment and fracture width. Figure 22 shows the simulated figure of the fracture width under a 2.75–3.75 mm segment misalignment.

As shown in Figure 22, when the amount of misalignment reaches 3.75 mm, the simulated value of the fracture width is 0.22 mm, exceeding the standard limit value by 0.2 mm. When the amount of misalignment increases from 2.75 mm to 3.75 mm, the rate of increase in the fracture width increases rapidly, and the slope of the curve increases from 0.04 to 0.36. As shown in Figure 22, the maximum fracture width occurs in the 9 o'clock part of the segment.

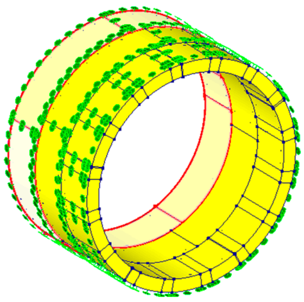

Figure 20. Staggered ring and constraint ring.

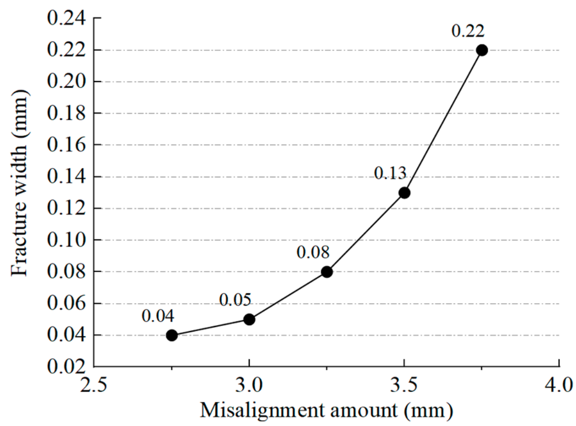

Figure 21. Plot of segment misalignment and fracture width.

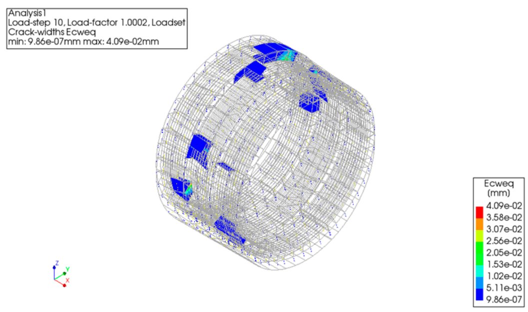

(**a**) Misalignment amount is 2.75 mm.

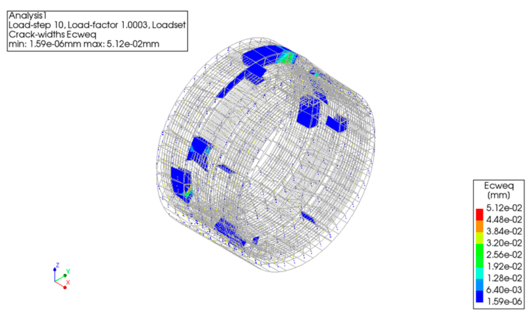

(**b**) Misalignment amount is 3 mm

Figure 22. *Cont.*

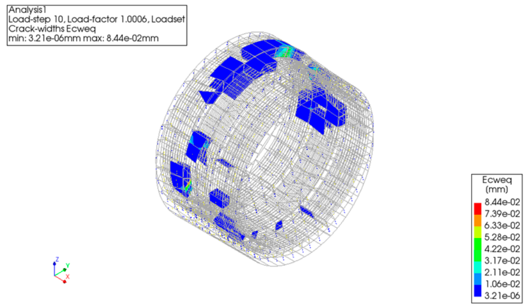

(**c**) Misalignment amount is 3.25 mm

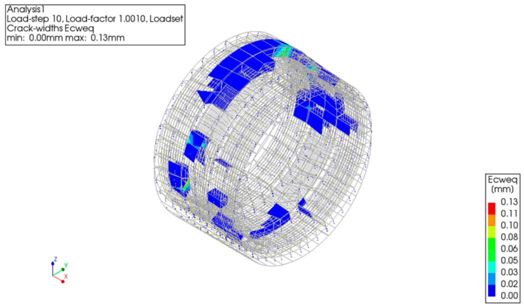

(**d**) Misalignment amount is 3.5 mm

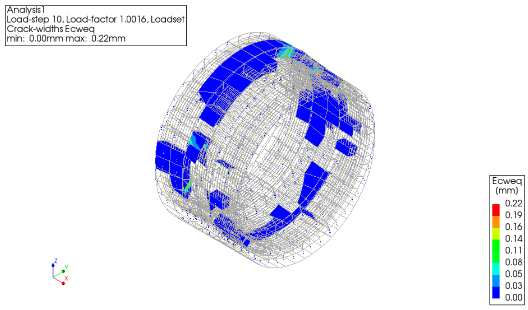

(**e**) Misalignment amount is 3.75 mm

Figure 22. Numerical simulation figure of fracture width under 2.75–3.75 mm misalignment of segment.

5. Discussion

In this paper, the Rots model from the finite element software Diana was used to calculate the crack width in concrete segments, and combined with field measurements, the cracking mechanism of concrete segments under external loads such as jack thrust deflection angle or uneven jack thrust caused by the changes in the segment's upward buoyancy and shield attitude were studied, and cracking conditions and engineering control measures of concrete segments were summarized. The influence of jack thrust, thrust direction change, cylinder pressure non-uniform allowance and buoyancy on segment crack width was investigated and compared with engineering practice. Based on this, the empirical formula of segment crack in Japan's "Code for Shield Tunnel Segment Design" was optimized to provide research basis for similar projects. The numerical simulation results in this paper can show the crack location and crack width accurately, but cannot provide the crack trend, which needs further study.

6. Conclusions

In this paper, a numerical model was established according to actual tunneling conditions to investigate the effects of jack thrust, thrust direction change, nonuniform distribution of cylinder pressure and segment misalignment on segment fracture width when the tunnel segment is designed with an outer diameter of 6.2 m and an inner diameter of 5.5 m and the shield machine uses 16 grippers with an area of 0.1 m^2 for propulsion. The following conclusions are drawn, and measures to prevent the segment fracture width from exceeding the allowable value during shield tunneling are proposed:

(1) The empirical formula of segment fracturing in the Japanese Code for the Design of Segments for Shield Tunnels is optimized. The empirical formula does not provide a method to solve the increase in stress of the steel bar; The maximum stress at the fracture of the segment is used instead.
(2) When the attitude of the shield and segment are exactly the same, the total thrust of the shield is recommended not to exceed 21,000 kN, and is strictly limited to 24,000 kN.
(3) When the inclination angle between the shield machine and the segment is less than 1°, the influence on the quality of the segment is small. When this inclination angle reaches 2°, the total thrust of the shield is recommended not to exceed 16,000 kN, and is strictly limited to 18,000 kN; when the inclination reaches 3°, a fracture is easily produced.
(4) When the total thrust is 16,000–19,000 kN, it is recommended that the loading increase or decrease in the left and right four grippers should not exceed 20–30%, and are prohibited to exceed 30–50%.
(5) The fracture width increases exponentially with increasing dislocation between adjacent segment rings. The maximum fracture width usually arises in the 9 o'clock part of the segment.

Author Contributions: Conceptualization, T.F. and X.Z.; methodology, C.Z.; software, B.Z.; validation, C.Z., B.Z. and G.R.; formal analysis, C.Z.; investigation, S.H.; resources, C.Z.; data curation, B.Z.; writing-original drift preparation, C.Z.; writing-review and editing, B.Z.; visualization, G.R.; supervision, X.Z.; project administration, T.F.; funding acquisition, T.F. All authors have read and agreed to the published version of the manuscript.

Funding: This research was funded by the National Natural Science Foundation of China (No.52378336).

Institutional Review Board Statement: Not applicable.

Informed Consent Statement: Not applicable.

Data Availability Statement: The data used to support the findings of this study are available from the corresponding author upon request.

Acknowledgments: This work was sponsored by the National Natural Science Foundation of China (No. 52378336). The authors are grateful to these institutions for their support.

Conflicts of Interest: Author Cheng Zhu was employed by the China Communications Construction Company. The remaining authors declare that the research was conducted in the absence of any commercial or financial relationships that could be construed as a potential conflict of interest.

References

1. Liu, X.; Feng, K.; Xiao, M.Q. Local prototype test of a new distributed tenon segment structure for shield tunnel. *Eng. Mech.* **2022**, *39*, 197–208. (In Chinese)
2. Tang, D.Y. Study on Influence of Cracking of Segment of Concrete on Performance and Control Measures. Ph.D. Thesis, (In Chinese). Guangxi University, Nanning, China, 2021. (In Chinese)
3. Jun, W.L.; Fei, X.; Tian, M.W. Research on the Evolution of Shield Segment Cracks Based on Acoustic Emission and CMOD. *Materials* **2022**, *15*, 5829. [CrossRef] [PubMed]
4. Ding, D. Research on Calculation Method of Fracture width of Reinforced Concrete Structure. Master's Thesis, Tianjin University, Tianjin, China, 2007. (In Chinese)
5. Saliger, R. *High Grade Steel in Reinforced Concrete. Preliminary Publication, 2nd Congress of IABSE*; Munich: Berlin, Germany, 1936.
6. Broms, B.B. Crack Width and Spacing in Reinforced Concrete Members. *ACI* **1965**, *62*, 1237–1256.
7. Broms, B.B.; Lutz, L.A. Effects of Arrangement of Reinforcement on Crack Width and Spacing of Reinforced Concrete Members. *ACI* **1965**, *62*, 1395–1410.
8. Gergely, P.; Lutz, L.A. Maximum crack width in reinforced flexural members. *ACI* **1968**, *20*, 87–117.
9. Yukimasa, G. Cracks Formed in Concrete Around Deformed Tension Bars. *J. Proc.* **1971**, *68*, 244–251.

10. *GB 50010-2010*; Industry Standard of the People's Republic of China. Code for Design of Concrete Structures. Building and Architecture Press: Beijing, China, 2010. (In Chinese)
11. Xu, Z.; Wang, T.; Chen, S.; Qian, H.; Liu, Y.; Yan, D. Unified models for bond strength and bond-slip response of deformed rebars in cracked concrete. *Constr. Build. Mater.* **2024**, *412*, 134806. [CrossRef]
12. Wei, Z. (Ed.) *Tunnel Standard Specification (Shield Chapter) and Interpretation: 2006*; China Architecture and Building Press: Beijing, China, 2011. (In Chinese)
13. Xu, F.; Xiao, Y.; Wang, S.; Li, W.; Liu, W.; Du, D. Numerical model for corrosion rate of steel reinforcement in cracked reinforced concrete structure. *Constr. Build. Mater.* **2018**, *180*, 55–67. [CrossRef]
14. Ezazi, M.; Hossaini, M.F.; Sheikhmali, R.; Khosrotash, M.; Teshnizi, E.S.; O'kelly, B.C. Assessment of steel-fiber-reinforced segmental lining of Chamshir water conveyance tunnel, Iran: Integrating laboratory experiments, field observations, and numerically analysis. *Case Stud. Constr. Mater.* **2024**, *20*, e03144. [CrossRef]
15. Liu, X.; Liu, Y.; Jiang, Z.; Wang, J.; Mang, H.A. Numerical investigation of the mechanical behavior of segmental tunnel linings reinforced by a steel plate—Concrete composite structure. *Eng. Struct.* **2023**, *276*, 115350. [CrossRef]
16. Yu, Y.; Hou, C.; Rabczuk, T.; Zhao, M. A coupling method between phase field model and classical linear elastic theory model for static and dynamic fracture. *Theor. Appl. Fract. Mech.* **2024**, *131*, 104432. [CrossRef]
17. Mesut, S. Nonlinear static and free vibration analysis of microbeams based on the nonlinear elastic foundation using modified couple stress theory and He's variational method. *Compos. Struct.* **2014**, *112*, 264–272.
18. Delfani, M.R.; Amadeh-Rajiri, S. Elastic and plastic fields induced by a screw dislocation in a nanowire within Mindlin's second strain gradient theory. *Appl. Math. Model.* **2022**, *109*, 77–97. [CrossRef]
19. Watanabe, O.; Atluri, S.N. Internal time, general internal variable, and multi-yield-surface theories of plasticity and creep: A unification of concepts. *Appl. Math. Model.* **1986**, *2*, 37–57. [CrossRef]
20. Jiang, Y.Y.; Li, L.; Hu, Y.J. Strain gradient viscoelasticity theory of polymer networks. *Int. J. Eng. Sci.* **2023**, *192*, 103937. [CrossRef]
21. Borges, J.G.O.; Karam, V.J. Elastic-viscoplastic analysis of plate bending with Reissner's theory by the Boundary Element Method. *Eng. Anal. Bound. Elem.* **2021**, *132*, 146–158. [CrossRef]
22. Suidan, M.; Schnobrich, W.C. Finite element analysis of reinforced concrete. *J. Struct. Div.* **1973**, *99*, 2109–2122. [CrossRef]
23. Bazant, Z.; Oh, B. Crack band theory for fracture of concrete. *Mater. Struct.* **1983**, *16*, 155–177.
24. Namdar, A.; Darvishi, E.; Feng, X. Effect of flexural crack on plain concrete beam failure mechanism: A numerical simulation. *Frat. Ed Integrita Strutt.* **2016**, *10*, 168–181. [CrossRef]
25. Lang, L.; Zhu, Z.M.; Zhang, X.S. Investigation of crack dynamic parameters and crack arresting technique in concrete under impacts. *Constr. Build. Mater.* **2019**, *199*, 321–324. [CrossRef]
26. Song, J. Analysis of Driving Attitude and Segment Damage Control of Shield Machine in Soft Soil Layer. Master's Thesis, Tsinghua University, Beijing, China, 2020. (In Chinese)
27. Ding, L.D.; Ding, X.T.; Yuan, C. Research on statistical model and standard value of concrete fracture energy. *J. Hebei Univ. Technol. (Nat. Sci. Ed.)* **2017**, *34*, 5–9. (In Chinese)
28. Xiao, Q.C. *Shield Tunnel Segment Design: From Allowable Stress Design Method to Limit State Design Method*; China Building Industry Press: Beijing, China, 2012. (In Chinese)